Available online at www.sciencedirect.com
SCIENCE DIRECT®
Journal of Hydrology 309 (2005) 191–209
Journal of Hydrology
www.elsevier.com/locate/jhydrol

Estimating discharge in rivers using remotely sensed hydraulic information

David M. Bjerklie[a,*], Delwyn Moller[b], Laurence C. Smith[c], S. Lawrence Dingman[a]

[a]Department of Earth Sciences, University of New Hampshire, Durham, NH, USA
[b]Jet Propulsion Laboratory, California Institute of Technology, Pasadena, CA, USA
[c]Department of Geography, University of California, Berkeley, CA, USA

Received 13 August 2003; revised 2 November 2004; accepted 26 November 2004

Abstract

A methodology to estimate in-bank river discharge exclusively from remotely sensed hydraulic data is developed. Water-surface width and maximum channel width measured from 26 aerial and digital orthophotos of 17 single channel rivers and 41 SAR images of three braided rivers were coupled with channel slope data obtained from topographic maps to estimate the discharge. The standard error of the discharge estimates were within a factor of 1.5–2 (50–100%) of the observed, with the mean estimate accuracy within 10%. This level of accuracy was achieved using calibration functions developed from observed discharge. The calibration functions use reach specific geomorphic variables, the maximum channel width and the channel slope, to predict a correction factor. The calibration functions are related to channel type. Surface velocity and width information, obtained from a single C-band image obtained by the Jet Propulsion Laboratory's (JPL's) AirSAR was also used to estimate discharge for a reach of the Missouri River. Without using a calibration function, the estimate accuracy was +72% of the observed discharge, which is within the expected range of uncertainty for the method. However, using the observed velocity to calibrate the initial estimate improved the estimate accuracy to within +10% of the observed. Remotely sensed discharge estimates with accuracies reported in this paper could be useful for regional or continental scale hydrologic studies, or in regions where ground-based data is lacking.

Keywords: Remote sensing of river discharge; River channel hydraulics; Synthetic aperture radar; Discharge estimates from water-surface velocity; Discharge estimates from channel width and slope

1. Introduction

The development of methods to estimate the discharge of rivers using remotely sensed data would provide the means to increase the streamflow measurement network globally. This component of the land-surface water-budget is currently measured at ground-based gaging stations for many of the larger

* Corresponding author. Present address: US Geological Survey, 101 Pitkin Street, East Hartford, CT 06108, USA. Tel.: +1 860 291 6770.
E-mail addresses: dmbjerkl@usgs.gov (D.M. Bjerklie), delwyn.k.moller@jpl.nasa.gov (D. Moller), lsmith@geog.ucla.edu (L.C.Smith), ldingman@cisunix.unh.edu (S.L. Dingman).

0022-1694/$ - see front matter © 2004 Elsevier B.V. All rights reserved.
doi:10.1016/j.jhydrol.2004.11.022

rivers in populated regions, however large rivers in remote areas and small to intermediate sized rivers over much of the globe are not currently monitored (Alsdorf et al., 2003). Additionally, the global river-gaging network and access to these data have been decreasing in recent years (Vörösmarty et al., 1999; IAHS, 2001). Because of these trends, the current ground-based streamflow-gaging network does not provide adequate spatial coverage for many scientific and water management applications, including verification of the land-surface runoff contribution to the oceans and the spatial distribution of intra-continental runoff.

Calibration of continental scale runoff models will depend on adequate spatial density and length of streamflow records. Remote sensing of river discharge has the potential to provide this needed data by filling in gaps within the existing streamflow-gaging network, and by adding new information from inaccessible regions that have not been gaged in the past. The use of remotely sensed information to track changes in river discharge has been shown to be feasible and potentially useful where ground-based data is difficult to obtain (Kuprianov, 1978; Koblinsky et al., 1993; Birkett, 1998; Brakenridge et al., 1994, 1998; Horritt et al., 2001, Birkett et al., 2002). These studies suggest that remotely sensed river hydraulic data could be used to directly estimate the discharge at a specific location, if ground-based discharge measurements are used to develop discharge ratings in conjunction with the remotely observed variable(s).

The advantage of using remote sensing is that it has the capability to provide information over large areas including those that are difficult to access from the ground. Thus, there is a need to develop estimation strategies that do not require ground-based information at all locations. For this reason, site specific discharge ratings developed from ground-based flow measurements and remotely sensed hydraulic information are not practical unless the discharge ratings are transferable to areas where ground measurements of flow are not available.

Estimating discharge in rivers from hydraulic information obtained solely from aerial and satellite platforms has been explored and summarized by Smith et al. (1996), Smith (1997) and Bjerklie et al. (2003). The water-surface width (estimated from water-surface area), channel slope and mean channel width (estimated from channel-surface area) can all be obtained from existing remote sources. The surface velocity of rivers can also be observed remotely using various forms of Doppler radar or lidar. Bjerklie et al. (2003) has suggested that these data can be used to estimate in-bank river discharge using various general hydraulic equations.

This paper applies a methodology, based on the hydraulic relationships described by Bjerklie et al. (2003), to estimate in-bank river discharge using remotely sensed width information and channel slope obtained from topographic maps. The use of water-surface velocity observed from SAR imagery as an additional predictor variable is also explored. The results of these applications contribute to an assessment of the data requirements and potential accuracy of space-based discharge estimating methods.

2. Images and remote data

River reaches selected for analysis were located at or near established river gaging stations so that measured discharge values were available for comparison with estimates made from the remotely sensed data. Mean daily discharge observations were obtained from the USGS National Water Information System (NWIS) on-line database or from the Water Survey of Canada (Smith et al., 1996). Although the discharge estimates made from the remote data strictly only apply to the moment when the remote observation was made, it is assumed that the mean daily discharge is nearly equivalent to the instantaneous discharge at the time of the remote observation.

Fourteen air photos, taken as part of the National Aerial Photography Program (NAPP), were obtained from the USGS Earth Resource Observations Systems (EROS) Data Center for analysis. The photos depicted the channel reach of seven different rivers in New England near the corresponding USGS gaging station on each river during different flow conditions, generally in the low range of discharge relative to the mean annual flood. These photos are georeferenced and routinely taken as part of the USGS topographic mapping program. The photos were printed at a scale of 1:10,000. The mean water-surface width and mean maximum channel width

were measured by averaging at least 20 equally spaced sections perpendicular to the channel banks over a reach length of not less than two meander lengths and more than 10 times the width.

Eleven digital orthophoto quadrangles (DOQs) available from the National Digital Orthophoto Program (NDOP), showing the selected river reach in nine large rivers, were also obtained from the EROS data center for analysis. The resolution of the DOQs is 1 m. The water-surface width and maximum channel widths were measured from the DOQs by delineating the total water-surface and channel-surface areas within the reach by defining the area of interest within a series of polygons. The polygons were fit as closely as possible to the observed boundaries, and then the total area of the polygons summed and divided by the total reach length to obtain the mean width estimate.

The maximum channel width measured from the aerial photos and the DOQs was assumed to be the active channel (Fig. 1), identified by the presence of sand and gravel bars, marked changes in vegetation on the channel banks (typically sparse) that suggest a riparian zone with frequent inundation, and areas where recent scour or deposition could be observed. Islands with prominent point bars and sparse riparian vegetation were included in the maximum width. Islands with stable vegetation and areas that appeared to be old meander scars or scars from scour were not included. In some cases, the maximum channel width was not an obvious feature and a certain amount of operator judgment was required to define its extent. Thus, determination of the maximum channel width is a source of operator error. Comparing the channel surface area delineated for the Missouri River and the Sacramento River in Fig. 1, this source of operator error is most likely to be greater in highly active and irregular channels.

The localized variability is minimized by using aerial mean averages of width (and other variables) that more closely approximate the mean conditions in a channel, thus defining the appropriate reach length is a key element of the data collection. Leopold et al. (1964) and Leopold (1994) suggest that mean values for determining channel geometry should be averaged over at least one meander length (typically 11 channel widths) because this length reflects the energy dissipation regime of the reach. Rosgen (1994) suggests that data be averaged over a minimum of two meander lengths in order to provide the most meaningful values. For this study, the widths were averaged over a reach length at least 10 times the width along at least one meander wavelength.

The channel slope for all of the river reaches was measured from the corresponding USGS 1:24,000 scale topographic map by measuring the channel length between consecutive contour lines (approximately 3 m contour interval). All of the images were obtained for river reaches at or near USGS stream gaging stations. The mean daily discharge for the day of each image was available for comparison with the discharge estimates made from the images. Flow conditions at the time of the observations in all of the rivers tended to be relatively low compared to the mean annual flood.

A time series set of SAR images obtained from ERS-1, were analyzed by Smith et al. (1996) to obtain the water surface area at different discharges in three large braided rivers (the Tanana and Taku Rivers in Alaska, and the Iskut River in British Columbia). The resolution of the images is 25 m with a processed pixel resolution of 12.5 m, and were collected at C-band. A total of 41 water surface areas were obtained for the three rivers, 19 for the Iskut, 11 for the Taku, and 11 for the Tanana. The water surface area estimates were made by summing all pixels classified as water based on an automated procedure developed by Smith et al. (1996). The procedure sets a threshold spectral return value which minimizes missed water area and avoids inclusion of non-contiguous patches. After the initial classification, a bimodal majority filter was applied to each image to reduce speckle. Smith et al. (1996) reports that human induced method error associated with the determination of the water-surface area was within 0.1–13%, with an average error of 3%. The total water-surface area within the braided channel system observed was divided by the valley length to obtain a mean or 'effective' water surface width for the reach. For more detail on these data and on the processing techniques used to extract the effective widths from the SAR images, please refer to Smith et al. (1996).

The reach lengths observed ranged from 9 to 16 km (approximately 20–30 times the effective width). The channel slope was assumed to be represented by the valley slope for the braided rivers, and was measured from topographic maps. A maximum

channel width was not specifically measured by Smith et al. (1996). The maximum water-surface width from the time series was assumed to represent the maximum channel width for the purposes of the analysis presented here. In each river, the maximum observed width occurred during high flow conditions, and likely reflects a high flow event that is near the mean annual flood.

An airborne along track interferometric (ATI) SAR imager (AirSAR), flown by JPL, obtained an image of

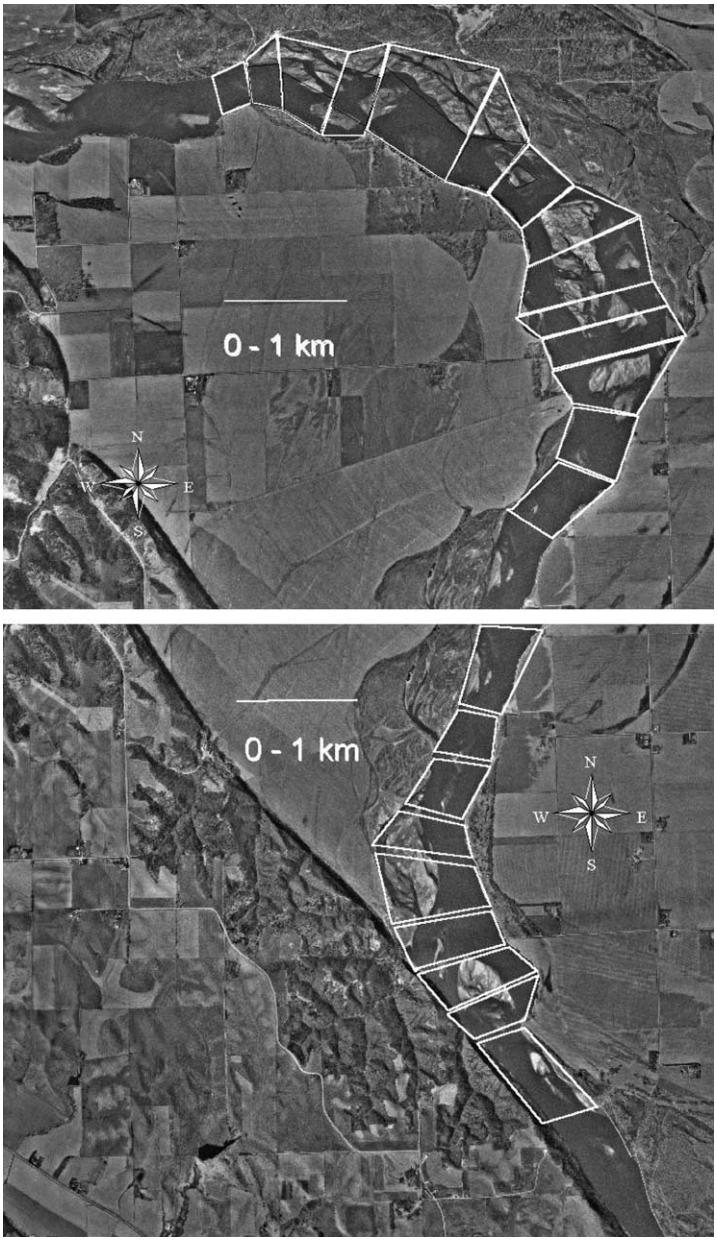

Fig. 1. Missouri River near Elk Point, SD (upper and middle panels) and Sacramento River near Red Bluff California (lower panel), showing digitized polygons delineating the maximum channel surface area (Source: 3.75 min DOQs for Elk Point (top) and Ponca (middle) South Dakota; and for Bend, California (lower), National Digital Orthophoto Program (NDOP)).

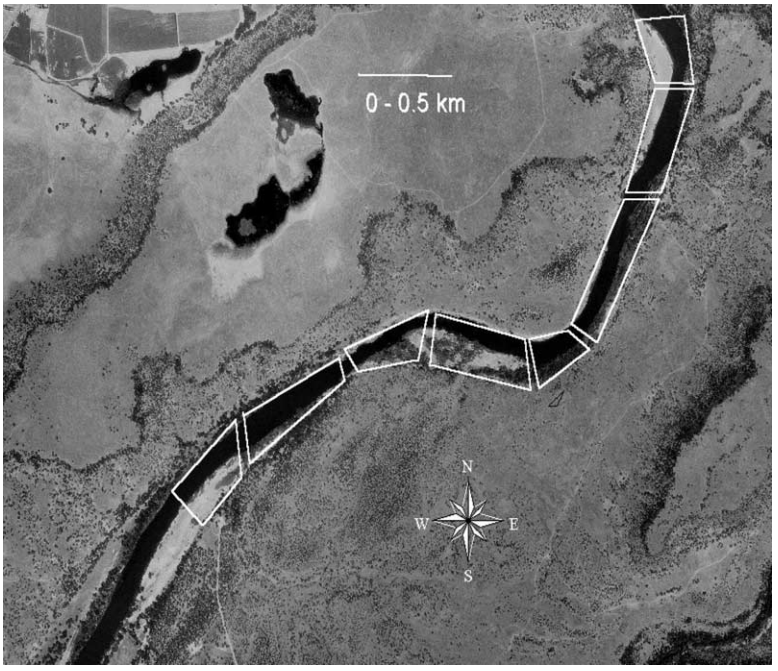

Fig. 1 (*continued*)

the Missouri River near Elk Point, SD on March 25, 2002 (Fig. 2). The resolution of the image depicted in Fig. 2 has been averaged to a resolution of 13 by 15 (slant range) and was collected at C-Band. The water-surface width and the surface velocity of the river were obtained from the image. The surface velocity was obtained using a Doppler along track interferometry technique developed by JPL (Goldstein et al., 1989). Fig. 2 shows the AirSAR radial velocity estimate projected onto the water surface. Note that in this figure positive velocities are flowing away from the radar to the South.

The velocities have also been corrected for the Bragg-resonant effect (Bragg, 1913) whereby short wind-driven waves on the river surface have the effect of biasing the velocity estimate by their phase speed (Kinsman, 1965). In this case the Bragg velocity is approximately 0.23 m s^{-1} although the correction increases with range due to the increasing incidence angle. At the time of the image, a mild wind (approximately 5 m s^{-1}) was inferred from the nearby weather station in Sioux City, IA to be blowing in the direction of the river flow. Given the flat topography of the landscape it is reasonable to assume that the wind direction in the imaged area will be consistent with the weather station's observation. Therefore the South-bound wind has the effect of biasing the velocities high indicating that subtracting the Bragg phase-speed was necessary.

Because the ATI-SAR measures velocity in the radial direction only, the portion of the river which is oriented nearly parallel to the flight direction detects very low velocities (Fig. 2). As such, for this study we have chosen to analyze the region where the river is directed toward the radar. Techniques to alleviate this limitation will be introduced in Section 6 as an area of future development.

The slope of the river channel was obtained from USGS topographic mapping, and the approximate maximum channel width was measured from a recent DOQ of the same reach from (photo taken on April 4, 1993). The reach of river where the image was taken is characterized by large sand and gravel bars, and is much wider than both upstream and downstream

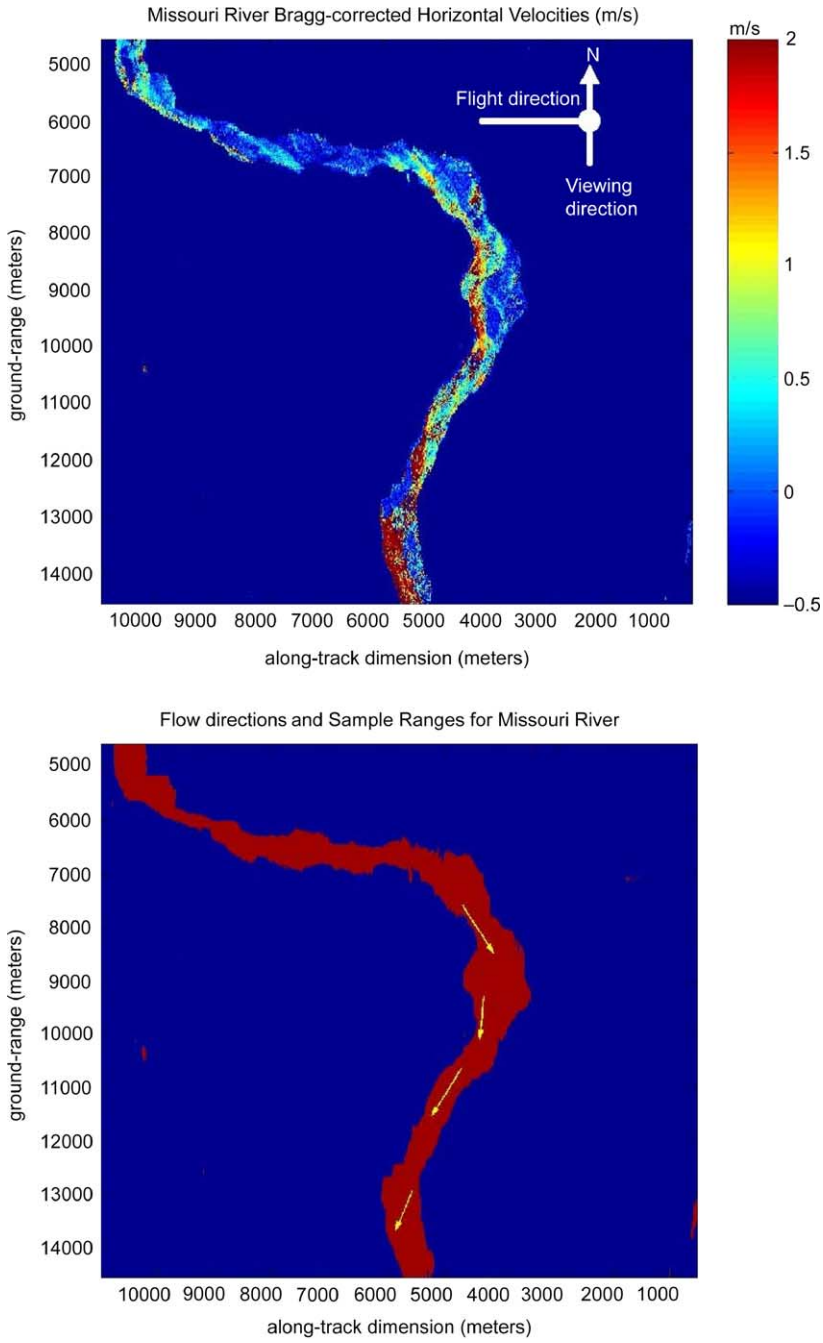

Fig. 2. The upper panel shows an image of the Missouri River near Elk Point, SD as collected by JPL's AirSAR at C-band using its along track interferometric capability to measure radial surface velocities. The image shows the measured velocities after being projected into the horizontal plane and corrected for the phase-speed of the Bragg-resonant waves. The radar viewing orientation was South with the aircraft flight direction from east to west. The lower panel shows the derived flow directions on a masked image (red, the river area and blue, the masked out surrounding land). Note that the flow directions are biased by the regions of high flow, especially given that the sandbar regions are neglected in the estimation process (source: JPL Air SAR).

sections of the river. This reach of river is considered a-typical, or non-conforming relative to the Missouri River in general in this region.

Because of several sand and gravel bars, estimating the effective water-surface width in the channel was problematic. We did not include areas where the measured surface velocity was below $0.15\ m\ s^{-1}$ because of the potential for higher inaccuracy in the velocity estimate. Additionally, taking this approach avoids potential complications associated with non-parallel flow lines, which would more likely be present over the shallow bars, and reduces the potential for assigning too much weight to flow regions that do not contribute significantly to the downstream flow. For this reason, the effective water-surface width was assumed to include only those regions where the surface velocity was greater than the threshold value. Thus, the areas where velocities were lower than the threshold were not included in the estimates of mean velocity and river width.

The number of river pixels excluded at this threshold was 14.3%. It was qualitatively found that the mean velocity estimates and the effective water-surface widths across the channel were relatively insensitive to the chosen threshold except in the region of one large sand and gravel bar. Selecting a threshold value of $0.15\ m\ s^{-1}$ effectively excluded the large sand and gravel bar, while minimizing the exclusion of pixels from the remainder of the scene. Ideally an algorithm that is more generic based on the statistics of the scene might be developed. The maximum active channel width was also evaluated from the AirSAR image. The active channel width was masked by including in the channel area all pixels that showed distinctly lower brightness than surrounding land areas. However, some of the included areas were not considered to be part of the active channel based on inspection of the DOQ image for the same reach. These areas are considered to be old meander and braid scars that have not been fully re-vegetated relative to the land. Manually excluding these areas results in an active channel mask with a mean width of 655 m with a standard deviation of ± 118 m, which is very close to the value determined from the DOQ.

A mean cross-channel width and velocity were determined for four portions of the observed river reach that were oriented towards the radar, and which were able to provide reliable estimates of both width and velocity. Vector velocity estimates were inferred from the radial velocities by assuming that the direction of flow was parallel to the river direction. Fig. 2 shows the inferred direction of flow and regions of the river that were used to obtain four discharge estimates. The river lengths were constant in radar range but varied in absolute range depending on the estimated direction of flow. Note that the flow direction estimates in Fig. 2 are biased toward the high-flow regions and exclude the obvious sandbars (compare with upper frame of Fig. 2). The absolute ranges were [1107, 765, 976, 730] m, respectively (from north to south) while the estimated water-surface width (adjusted for the direction of flow and excluding sand-bar regions) was 330 m on average (as previously mentioned velocities $<0.15\ m\ s^{-1}$ were excluded from the estimation process). Although the range to width ratio is quite low, this was necessitated by the assumption that the river flow is parallel to the banks, requiring that the channel be relatively 'straight' over the lengths evaluated.

The accuracy of the water-surface and maximum channel width estimates measured from the images are, in part, a function of the resolution of the images and the accuracy of the measuring tool. Thus, the resolution of the DOQs (1 m) and the SAR images (10 m ERS-1 SAR, and 5 m JPL AirSAR) indicate the accuracy of an estimated width measurement if it were a single measured value. However, the widths were estimated by measuring the total water-surface area of the reach divided by the reach length. This procedure would necessarily improve the accuracy of the estimate due to the effect of averaging. However, the methods used to measure the surface area may introduce additional unknown error. In the case of the NAPP aerial photos, the image resolution is a function of the ability to sharply see the boundary of the defined object (since these are not digital). We estimated that the width measurements made from these photos at 1:10,000 scale is approximately 4 m, however the width estimates measured from these photos was also an average of many measured widths. Thus, the accuracy of the width estimates made from the various images is not precisely known. Because of the effect of averaging and resolution, the accuracy of the width measurements would generally be greater for larger rivers.

3. Discharge estimating methodology

Generally applicable open-channel hydraulic equations, including the Manning and Chezy equations, have been in use for decades, and can be adapted to remote sensing applications because the dynamic constitutive elements of the equations can all be measured or potentially measured remotely, provided a general estimate of the resistance can be made. Bjerklie et al. (2003) used multiple regression analysis to statistically derive a general resistance equation similar to the Manning equation that uses observable river channel hydraulic information to estimate in-bank discharge in rivers. The form of the equation is modeled on the resistance equation as formulated by Chezy and Manning that relates discharge to width, depth, and slope as a power function. As previously stated the slope is taken to be the topographic channel slope, and is thus a geomorphic constant for each river reach. The relation was calibrated and validated on a database of discharge measurements ($N=1012$), and is given as:

		r^2	std. error	
Model 1:	$Q = 7.22W^{1.02}Y^{1.74}S^{0.35}$	0.95	0.23	(1)

where W is the water-surface width (m), Y is the average water depth (m), V is the average water velocity (m s^{-1}), and S is the channel slope measured from 1:24,000 scale topographic maps.

Model 1 minimizes the variance associated with channel resistance by maximizing the variance explained by measurable (and observable) geometric and hydraulic channel variables. It can be expected to provide discharge estimates, on average, within 20% of the ground-measured value, with the standard error within a factor of 1.5–2 (50–100%). The data used to calibrate and validate Model 1 included in-bank river discharge measurements from more than 100 single channel rivers. Most of the river channels in the database were located in relatively straight reaches conducive to on-the-ground measurements. Because of this, different discharge coefficients would be expected in non-conforming reaches such as braided channels, channel reaches that are not 'typical' for the river system being observed, and reaches where slope is controlled by a hydraulic feature such as a dam or canyon.

Model 1 is similar to the well known Manning equation, given as:

$$Q = WY^{1.67}S^{0.5}/n \tag{2}$$

where n is the Manning resistance coefficient in that the exponents on the width and depth variables (assuming mean depth to be equivalent to the hydraulic radius) are not significantly different at the 95% confidence level to those defined by Manning (1889). The exception is that the slope exponent defined by Manning is 0.5 rather than 0.34. Based on the statistically derived Model 1, we suggest that a general form for natural rivers be defined as:

$$\text{Model 1 (general)}: \quad Q = k_1 WY^{1.67}S^{0.33} \tag{3}$$

with the coefficient k_1 representing a general conductance coefficient (rather than a resistance). The exponent on the width (1.0) and the depth (1.67) terms in Eq. (3) are within the 95% confidence level of Eq. (1). The proposed slope exponent of 0.33 can be derived if the resistance is assumed to be proportional to $S^{0.17}$, as suggested by Lacey (1946–1947) and Bray (1979).

Bjerklie et al. (2003) also proposed and statistically developed two other discharge estimation models that use velocity rather than depth as a predictor. The form of these models were given as:

$$\text{Model 2}: \quad Q = k_2 W^p V^q S^r \tag{4}$$

$$\text{Model 3}: \quad Q = k_3 W^s V^t \tag{5}$$

A general form of Model 2 can be developed by solving for Y in Eq. (3) and then substituting this into the equation of continuity ($Q=WYV$) to yield:

$$\text{Model 2 (general)}: \quad Q = k_2 WV^{2.5}S^{-0.5} \tag{6}$$

A general form of Model 3 can be derived independently based on principles of hydraulic geometry (Leopold et al., 1964), which recognizes the general relationship between mean depth and discharge ($Y=cQ^x$) in a given channel reach (at-a-station) and between channel reaches in the same river and between rivers (down-the-channel). The value of x for both at-a-station and down-the-channel hydraulic geometry relations, as measured in various

rivers, can generally be approximated by a value of 0.4 depending on the condition of the banks (Leopold et al., 1964; Dingman, 1984). Because its value for both at-a-station and down the channel hydraulic geometry is similar, it is suggested that using $x=0.4$ would be generally applicable for a diverse set of rivers. Assuming the validity of the hydraulic geometry concept, Model 3 can be derived by substituting $cQ^{0.4}$ for Y into the equation of continuity and re-arranging. The resulting general form of Model 3 is:

$$\text{Model 3 (general)}: \quad Q = k_3 W^{1.67} V^{1.67} \tag{7}$$

Suitable values for k_1, k_2, and k_3 were determined from a large database of observed flow measurements ($N=1037$) from 103 rivers in the United States and New Zealand (obtained from Barnes (1967), Hicks and Mason (1991), Coon (1998) and the US Geological Survey's (2001) on-line NWIS flow measurement database (USGS, 2001)). The channel slope assigned to each river in the database was obtained from topographic maps or as an average of all measured values (comparable to the slopes obtained for the image analysis). All of the rivers represented in the database are single channel and do not exhibit any control on the channel slope such as large expansions or contractions within the reach where the data was collected. This channel selection criteria was implemented so that the hydraulic variables could all be considered adjusted to the channel slope. A constant coefficient values was determined for each model by minimizing the mean of the log-residuals for the entire database assuming the defined exponents. The resulting values are $k_1=7.2$, $k_2=0.05$, and $k_3=0.1$. The standard deviation of the log residuals are comparable to the standard error of the regressions determined for the similar models developed statistically by Bjerklie et al. (2003).

With the exception of the AirSAR image (which includes surface velocity), the remote data sources provide water-surface area (mean water-surface width), channel area (mean channel width), and channel slope information. Combining Models 2 and 3 with the calibrated values for k_2 and k_3 and re-arranging to solve for velocity gives:

$$V = 2.3 W^{0.8} S^{0.4} \tag{8}$$

This equation is used to estimate the mean velocity from the water-surface width and slope. However, combining these models compounds the error associated with each model. Bjerklie et al. (2003) has shown that statistically derived models of this type have an estimate bias in the same direction, and that the standard deviation of the estimate error using these models would be expected to be within a factor of 1.5–2 times the actual value. Thus, Eq. (8) would be expected to yield relatively large estimate errors. This is especially true of the braided rivers, which were not represented in the calibration data, and which would not be expected to exhibit similar hydraulic relationships as the single channel rivers (Henderson, 1966).

Because of these issues, a calibration method is employed that uses measured geomorphic variables (maximum channel width and the channel slope) to predict a discharge correction factor. The calibration functions are developed from the remotely sensed data sets presented herein, and therefore are not independent of ground-based discharge information. However, the calibration functions suggest a methodology that can be expanded to include larger data sets such that more robust functions can be developed, and lead to a general understanding of method accuracy in rivers where observed discharge is not available.

4. Results

Estimates of discharge were developed from aerial photos and SAR imagery for which only width and slope data were available for all of the images described in Section 2. An estimate of discharge was also made and for the case where width, slope, and surface velocity were available from the AirSAR image.

4.1. Discharge estimates using width and slope

Initial estimates of discharge were made for the single channel data (Fig. 3a) and separately for the braided channel data (Fig. 4a). The results, as expected, are poor with large mean uncertainty, especially for the braided rivers. The discharge correction factor was then calculated as the observed discharge

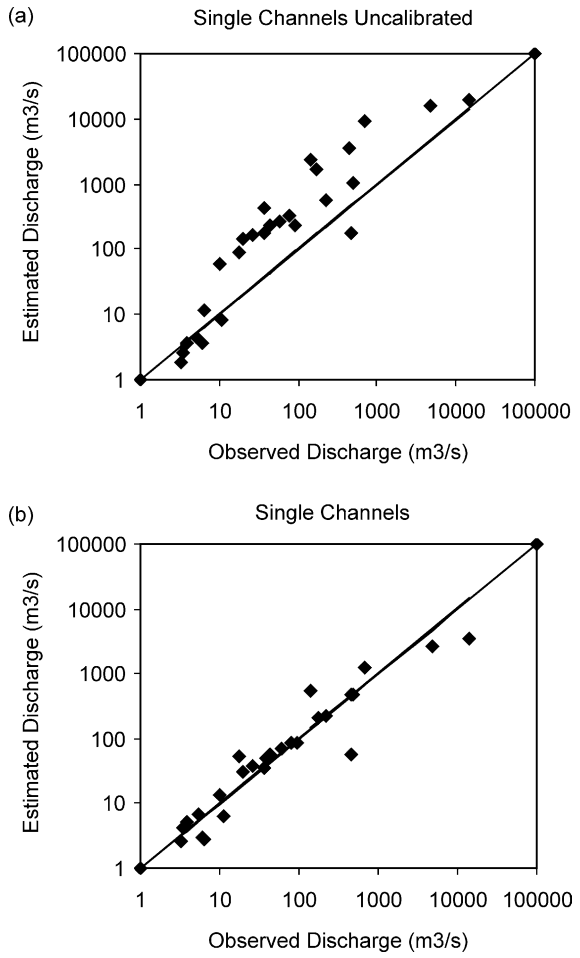

Fig. 3. Graph (a) shows the estimated initial discharge for the single channel rivers plotted against the observed discharge. Graph (b) shows the estimated discharge after correction using the calibration function plotted against observed discharge for the single channel rivers.

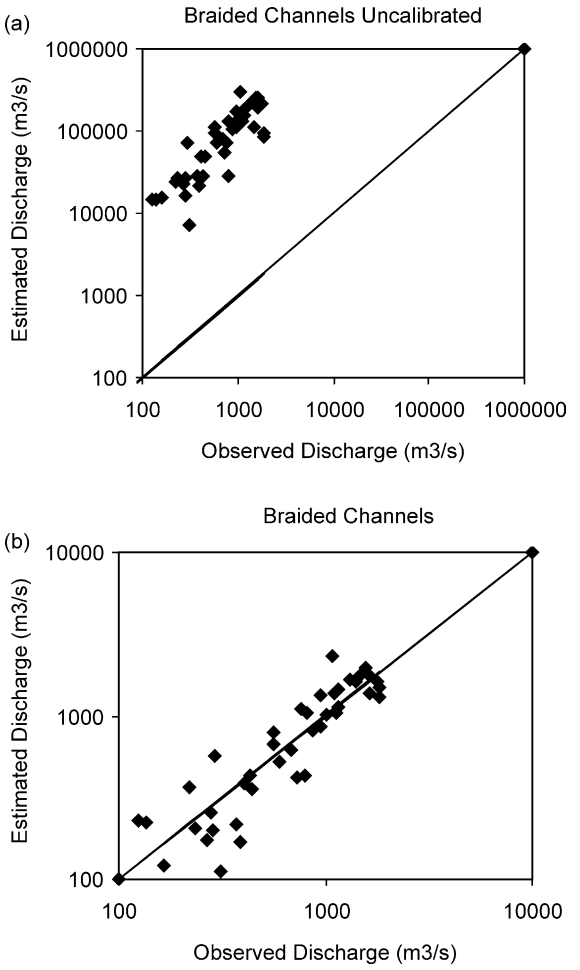

Fig. 4. Graph (a) shows the estimated initial discharge for the braided channel rivers plotted against the observed discharge. Graph (b) shows the estimated discharge after correction using the calibration function plotted against observed discharge for the braided channel rivers.

divided by the estimated discharge (Q_o/Q_e). This factor was then related to the observed maximum channel width and the channel slope as a power function using multiple regression analysis. The discharge correction (calibration) function was independently determined for the single channel data and the braided channel data. The resultant functions are:

		N	Std. error	
Single Channel:	$C = 0.13 W_m^{-1.26} S^{-0.98}$	26	0.32	(9)
Braided Channel:	$C = 2713 W_m^{-2.48} S^{-0.57}$	41	0.17	(10)

The large difference in the exponent and coefficient between the single channel and braided channel data sets indicates that using a general channel typing scheme is important to developing appropriate calibration functions. This would not be surprising, as mean values of depth and velocity, averaged across the braided channel system (i.e. the water-surface area) reflect different dynamics and flow regime compared to single channel systems (Henderson, 1966; Ferguson, 1986).

Table 1 lists the observed data, the initially estimated discharge, the correction factor and the corrected estimated discharge for the single channel rivers along with the mean and standard deviation of the estimate uncertainty expressed as the log residual ($\log(Q_o/Q_e)$ and the actual relative residual ($[Q_e-Q_o]/Q_o$). Table 2 shows the same data for the braided channel rivers. The corrected discharge estimates are also plotted against the observed discharge in Figs. 3b and 4b. As can be seen, the discharge correction greatly improves the estimates, and is essential to obtaining reasonable estimate accuracy.

The standard deviation of the residuals for the corrected discharge is less for the braided rivers compared to the single channel rivers. This suggests that the braided rivers constitute a more homogeneous data set, and also suggests that grouping the single-channel rivers by channel type or other physically based hydraulic factor, would improve overall estimate accuracy using the estimation approach outlined here. Inspection of the single channel data (Table 1) shows that the largest estimate uncertainty is associated with the Mississippi River at Thebes, IL and the Sacramento River near Red Bluff, CA. The river channels of both of these rivers are subject to management activities, which may account for their apparent anomalous behavior compared to the remainder of the data set. Removing these rivers and then determining a new calibration function results in better predictive statistics, with the mean and standard deviation of the log-residuals for the revised data set equal to 0.001 and 0.17, respectively, and for the relative residual +9 and 48%, respectively.

4.2. Discharge estimates using width, slope, and velocity

The SAR image obtained by JPL for the Missouri River provided both the surface velocity and water-surface width, enabling the use of Eq. (6) directly. The mean velocity in the vertical for the cross-section was estimated by applying a correction factor of 0.86 to the measured surface velocity (Rantz et al., 1982). Recent experiments by Costa et al. (2000) in several rivers in which surface velocity was measured using bank side and helicopter borne radar, this correction factor appears to provide reasonable estimates of mean velocity in the cross-section.

Table 3 (upper) provides the measured values of water-surface width and mean velocity in four relatively short sections of river within the observed reach. The nearest USGS gaging station on the Missouri River is located at Sioux City, IA, approximately 20 miles downstream of the observed reach. For the date of the SAR image, the discharge at this station was approximately 450 $m^3 s^{-1}$. There are no major tributaries entering the River between the observed reach and the gaging station at Sioux City, indicating that the discharge at Sioux City can be assumed to be approximately the same as for the observed reach. Eq. (6) was used to make the initial discharge estimates using the remotely measured width and velocity, and the channel slope.

The discharge estimates using Eq. (6) were approximately 70% higher than the observed discharge. These accuracies are within one standard deviation of the comparable statistical model (Model 2), which indicates that approximately 67% of the estimates would be within a factor of 2 (Bjerklie et al., 2003). Given that the reach is non-conforming compared to the database used to calibrate Eq. (6), the relatively large error is not surprising. As a comparison, the width and mean velocity for two discharge measurements made at the Sioux City gage on March 6 and March 13, 2002 with approximately the same discharge (442 and 476 $m^3 s^{-1}$, respectively) were 173 and 165 m for width, and 1.00 and 0.96 m s^{-1} for mean velocity. The channel slope at the gage is approximately the same as for the observed reach. Using Eq. (6) with these data provides estimates of discharge of 597 and 514 $m^3 s^{-1}$, respectively (errors of +35 and +8%).

Another approach to estimating the discharge is to use the measured surface velocity (converted to the mean velocity) as a correction factor rather than developing a calibration function from the observed maximum channel width and slope. The correction is made by computing the Froude number ($F=V/[(gL)^{0.5}]$, where the characteristic length L is taken to be the mean depth of flow Y, and g is acceleration due to gravity) from the initial discharge estimate, and then using the observed velocity to estimate the mean depth of flow from the computed Froude number. Using the estimated mean depth of flow and the observed width and channel slope, Model 1 is then used to compute a corrected discharge

Table 1
Hydraulic data and discharge estimate statistics for single channel rivers

River	Maximum channel width (m)	Channel slope	Water surface width (m)	Observed discharge ($m^3 s^{-1}$)	Initial estimates			Corrected estimates				
					Discharge estimate ($m^3 s^{-1}$)	Log residual	Relative residual	Actual correction factor	Predicted correction factor	Corrected discharge estimate ($m^3 s^{-1}$)	Log residual	Relative residual
Pemigewassett River at Plymouth, NH	82	0.0017	69.2	43	226.0	0.721	4.26	0.19	0.26	59.0	0.137	0.37
Pemigewassett River at Plymouth, NH	82	0.0017	78.6	78	331.1	0.628	3.25	0.24	0.26	86.4	0.045	0.11
Pemigewassett River at Plymouth, NH	82	0.0017	73.2	59	267.5	0.656	3.53	0.22	0.26	69.8	0.073	0.18
Pemigewassett River at Woodstock, NH	67.1	0.0026	54.6	26	169.8	0.815	5.53	0.15	0.22	37.6	0.160	0.45
Pemigewassett River at Woodstock, NH	67.1	0.0026	51.4	20	141.6	0.850	6.08	0.14	0.22	31.4	0.196	0.57
White River at West Hartford, VT	83.5	0.0012	78.6	93	233.7	0.400	1.51	0.40	0.36	83.9	−0.045	−0.10
Ammonoosuc River at Bethlehem, NH	27.9	0.0075	26.8	9.9	57.9	0.767	4.85	0.17	0.24	13.7	0.142	0.39
Ammonoosuc River at Bethlehem, NH	27.9	0.0075	15.7	6.4	11.6	0.260	0.82	0.55	0.24	2.8	−0.365	−0.57
Baker River near Rumney, NH	23.5	0.0013	19.9	5.4	4.1	−0.119	−0.24	1.31	1.64	6.7	0.096	0.25
Baker River near Rumney, NH	23.5	0.0013	16.9	3.5	2.5	−0.143	−0.28	1.39	1.64	4.1	0.072	0.18
Smith River at Bristol, NH	18.6	0.0037	17.7	11	8.2	−0.126	−0.25	1.34	0.79	6.5	−0.228	−0.41
Smith River at Bristol, NH	18.6	0.0037	13.6	6.1	3.7	−0.213	−0.39	1.63	0.79	2.9	−0.316	−0.52
Pomperaug River at Southbury, CT	18.4	0.0021	16.3	3.8	3.6	−0.018	−0.04	1.04	1.39	5.1	0.127	0.34
Pomperaug River at Southbury, CT	18.4	0.0021	13.1	3.3	1.9	−0.241	−0.43	1.74	1.39	2.6	−0.097	−0.20
Mississippi River at Thebes, IL	801	0.000137	710	14326	19669.1	0.138	0.37	0.73	0.17	3429.0	−0.621	−0.76
Mississippi River at Thebes, IL	801	0.000137	657	4700	15585.0	0.521	2.32	0.30	0.17	2717.0	−0.238	−0.42
Potomac River at Point of Rocks, MD	381	0.00027	280	144	2377.5	1.218	15.51	0.06	0.23	543.7	0.577	2.78
Missouri River near Elk Point, SD	651	0.00023	466	680	9336.3	1.138	12.73	0.07	0.14	1272.1	0.272	0.87

Missouri River near Elk Point, SD	651	0.00023	336	450	3499.7	0.891	6.78	0.13	0.14	476.8	0.025	0.06
South Platte River near Kersey, CO	125	0.00093	78	38	177.0	0.668	3.66	0.21	0.28	49.1	0.111	0.29
Missouri River near Culbertson, MT	343	0.000156	258	484	1074.7	0.346	1.22	0.45	0.45	480.3	−0.003	−0.01
Kansas River at Fort Riley, KS	115	0.00049	77	17.5	89.7	0.710	4.13	0.20	0.58	51.8	0.471	1.96
Sacramento R. below Bend near Red Bluff, CA	163	0.000575	92	459	179.6	−0.407	−0.61	2.56	0.32	57.1	−0.905	−0.88
Willamette River at Salem, OR	219	0.00032	164	221	566.2	0.409	1.56	0.39	0.39	220.2	−0.001	0.00
Delaware River at Port Jervis, DE	221	0.00098	162	172	1671.3	0.988	8.72	0.10	0.13	214.6	0.096	0.25
Wenatchee River at Monitor, WA	126	0.0032	69	37	421.7	1.057	10.40	0.09	0.08	34.5	−0.031	−0.07
Mean						0.458	3.65				−0.010	0.20
Standard deviation						0.473	4.30				0.307	0.77

estimate. The results of this procedure are shown in Table 3 (lower). The results show improved estimate accuracy, to within 10% of the observed discharge. This method for improving the discharge estimate is based on the observation that the Froude number is relatively stable even when the discharge estimates are highly variable.

Discharge estimates made using observed surface velocity in combination with measured width and channel slope eliminate the need to use maximum channel width as one of the predictor variables. This reduces the potential for errors resulting from the determination of this geomorphic variable, and makes the discharge estimation procedure more direct. Additionally, the need for the development of statistical calibration procedures is eliminated. However, conclusions regarding the potential accuracy of estimation methods using surface velocity cannot be made without additional data.

5. Evaluation of estimate errors

Sauer and Meyer (1992) present a methodology for evaluating the error associated with any individual measurement of discharge made by using the ground-based velocity–area method. Their analysis includes estimation of the standard errors associated with the physical measurement of each of the three elements of flow (width, depth, and velocity), and also errors associated with the measurement methodology. Method error includes instrument error, errors associated with measurement technique, and error associated with hydraulic assumptions (e.g. the assumption that either the 0.6 or average of 0.2 and 0.8 depth point velocity measurements represent the true mean velocity in a vertical profile). Sauer and Meyer (1992) suggest that errors associated with the ground-based measurement of width are negligible, thus the standard error of the discharge estimated is estimated as follows:

$$E_q = \sqrt{\left(\frac{E_y^2 + E_v^2}{N}\right) + E_m^2} \tag{11}$$

where E_q is the estimated standard error of the discharge measurement, E_y is the standard error of the depth measurement, E_v is the standard error of

Table 2
Hydraulic data and discharge estimate statistics for braided channel rivers

River	Maximum channel width (m)	Channel slope	Water surface width (m)	Observed discharge ($m^3 s^{-1}$)	Initial estimates			Corrected estimates				
					Discharge estimate ($m^3 s^{-1}$)	Log residual	Relative residual	Actual correction factor	Predicted correction factor	Corrected discharge estimate ($m^3 s^{-1}$)	Log residual	Relative residual
Iskut river	700	0.0022	437	292	73647	2.402	251.22	0.0040	0.0078	575	0.294	0.97
	700	0.0022	579	951	171296	2.256	179.12	0.0056	0.0078	1337	0.148	0.41
	700	0.0022	656	1570	249129	2.201	157.68	0.0063	0.0078	1945	0.093	0.24
	700	0.0022	584	1110	175772	2.200	157.35	0.0063	0.0078	1372	0.092	0.24
	700	0.0022	490	862	103825	2.081	119.45	0.0083	0.0078	810	−0.027	−0.06
	700	0.0022	393	735	53566	1.863	71.88	0.0137	0.0078	418	−0.245	−0.43
	700	0.0022	291	388	21747	1.749	55.05	0.0178	0.0078	170	−0.359	−0.56
	700	0.0022	261	164	15690	1.981	94.67	0.0105	0.0078	122	−0.127	−0.25
	700	0.0022	316	370	27847	1.877	74.26	0.0133	0.0078	217	−0.231	−0.41
	700	0.0022	621	1320	211343	2.204	159.11	0.0062	0.0078	1650	0.097	0.25
	700	0.0022	596	1140	186832	2.215	162.89	0.0061	0.0078	1458	0.107	0.28
	700	0.0022	498	948	108993	2.061	113.97	0.0087	0.0078	851	−0.047	−0.10
	700	0.0022	694	1080	294979	2.436	272.13	0.0037	0.0078	2303	0.329	1.13
	700	0.0022	533	1121	133627	2.076	118.20	0.0084	0.0078	1043	−0.031	−0.07
	700	0.0022	534	818	134380	2.216	163.28	0.0061	0.0078	1049	0.108	0.28
	700	0.0022	446	681	78292	2.061	113.97	0.0087	0.0078	611	−0.047	−0.10
	700	0.0022	311	235	26546	2.053	111.96	0.0089	0.0078	207	−0.055	−0.12
	700	0.0022	294	266	22426	1.926	83.31	0.0119	0.0078	175	−0.182	−0.34
	700	0.0022	381	403	48808	2.083	120.11	0.0083	0.0078	381	−0.024	−0.05
Taku river	580	0.0015	301	277	16409	1.773	58.24	0.0169	0.0155	254	−0.038	−0.08
	580	0.0015	358	436	27608	1.802	62.32	0.0158	0.0155	427	−0.009	−0.02
	580	0.0015	541	1840	95274	1.714	50.78	0.0193	0.0155	1475	−0.096	−0.20
	580	0.0015	520	1840	84604	1.663	44.98	0.0217	0.0155	1310	−0.148	−0.29
	580	0.0015	360	801	28073	1.545	34.05	0.0285	0.0155	435	−0.266	−0.46
	580	0.0015	229	309	7226	1.369	22.38	0.0428	0.0155	112	−0.441	−0.64
	580	0.0015	339	221	23441	2.026	105.07	0.0094	0.0155	363	0.215	0.64
	580	0.0015	288	136	14373	2.024	104.69	0.0095	0.0155	223	0.214	0.64
	580	0.0015	290	124	14675	2.073	117.35	0.0084	0.0155	227	0.263	0.83
	580	0.0015	574	1480	113793	1.886	75.89	0.0130	0.0155	1762	0.076	0.19
	580	0.0015	491	765	71224	1.969	92.10	0.0107	0.0155	1103	0.159	0.44

Tanana river	865	0.001	820.2	1764	221334	2.099	124.47	0.0080	0.0072	1602	−0.042	−0.09
	865	0.001	782.1	1617	191901	2.074	117.68	0.0084	0.0072	1389	−0.066	−0.14
	865	0.001	733.3	1158	158174	2.135	135.59	0.0073	0.0072	1145	−0.005	−0.01
	865	0.001	562.2	595	71279	2.078	118.80	0.0083	0.0072	516	−0.062	−0.13
	865	0.001	494.4	445	48476	2.037	107.93	0.0092	0.0072	351	−0.103	−0.21
	865	0.001	407.9	283	27224	1.983	95.20	0.0104	0.0072	197	−0.157	−0.30
	865	0.001	614.6	566	93125	2.216	163.53	0.0061	0.0072	674	0.076	0.19
	865	0.001	704.8	1000	140439	2.147	139.44	0.0071	0.0072	1017	0.007	0.02
	865	0.001	825.9	1413	225981	2.204	158.93	0.0063	0.0072	1636	0.064	0.16
	865	0.001	857.7	1586	253102	2.203	158.59	0.0063	0.0072	1832	0.063	0.16
	865	0.001	649.1	561	109704	2.291	194.55	0.0051	0.0072	794	0.151	0.42
Mean						2.030	118.59				−0.006	0.06
Standard deviation						0.219	52.94				0.169	0.40

the velocity measurement, E_m is the standard error for the method, and N is the number of discrete velocity and depth measurements made across the measurement section.

This same approach can be applied to the estimation of the standard error for a discharge measurement made using remotely sensed information. Using Eq. (3), the comparable error equation would be:

$$E_q = \sqrt{E_w^2 + E_h^2 + E_m^2} \tag{12}$$

where E_w is the standard error associated with the measurement of width (not negligible when measured remotely) and E_h is the error associated with the slope. The model standard error (E_m) is assessed after application of the calibration function.

Bjerklie et al. (2003) determined the standard error (E_m) for the general models used here for Eqs. (3) and (6) using a map derived slope, and ground measured values for width and other hydraulic variables. Thus, slope measurement error would be included in the standard error associated with the modeling and thus equation would reduce to:

$$E_q = \sqrt{E_w^2 + E_m^2} \tag{13}$$

If surface velocity measurements were used the standard error would include the measurement error associated with the surface velocity measurement (E_v) and the error associated with estimating mean velocity from surface velocity (E_{va}), given by:

$$E_q = \sqrt{E_w^2 + E_v^2 + E_{va}^2 + E_m^2} \tag{14}$$

The additional measurement errors could be offset by a reduction in the modeling error.

Sauer and Meyer (1992) indicate that E_q for a ground-based velocity–area measurement would typically range between 2 and 10% not including unknown error associated with measurement site selection and other operator based decisions. Thus, the actual standard error for a discharge measurement may be somewhat greater than their reported range. A full evaluation of the errors associated with estimating discharge from remotely sensed information will require the development of larger data sets of remotely measured variables, however if we accept

Table 3
SAR image Missouri river near Elk Point, SD

Discharge estimates using Eq. (3)

Cross-section	Width (m)	Surface velocity ($m\ s^{-1}$)	Estimated mean velocity ($m\ s^{-1}$)	Channel slope	Estimated discharge ($m^3\ s^{-1}$)	Discharge at Sioux City ($m^3\ s^{-1}$)	Percent error
1	315	1.13	0.97	0.00023	966.8	450	114.9
2	313	1.07	0.92	0.00023	838.2	450	86.3
3	370	0.80	0.69	0.00023	478.9	450	6.4
4	321	1.05	0.90	0.00023	820.0	450	82.2
Average	330	1.01	0.87	0.00023	776.0	450.0	72.4

Discharge estimate using general discharge estimating procedure and velocity as correction factor

Cross-section	Estimated velocity ($m\ s^{-1}$)	Initially estimated discharge ($m^3\ s^{-1}$)	Estimated Froude number	Channel slope	Estimated depth (m)	Estimated discharge ($m^3\ s^{-1}$)	Percent error
1	1.50	2883.7	0.19	0.00023	2.53	672.9	49.5
2	1.50	2829.1	0.19	0.00023	2.28	562.7	25.0
3	1.71	4673.3	0.20	0.00023	1.20	227.5	−49.4
4	1.53	3051.6	0.20	0.00023	2.16	527.2	17.2
Average	1.56	3359.4	0.20	0.00023	2.04	497.6	10.6

estimates of E_w to be on the order of 5–10% (Smith et al., 1996), and the modeling error to be on the order of 50–100% (Bjerklie et al., 2003), application of Eq. (13) indicates that estimates of discharge made from remotely sensed information would also range between 50 and 100% due to the relatively small contribution to the standard error from the measured width variable.

Clearly, the model error associated with the remote estimate dominants the discharge error, and indicates that improvements in estimation models would yield the largest return in prediction accuracy. This is especially the case for large rivers because measurement precision is based on pixel resolution, which has a fixed dimensional value, and ability to accurately classify each pixel as water or not water. Thus, a 10 m error due to resolution would be a much smaller percent error if the river were 1000 m wide as opposed to a 100 m wide river, and similarly the effect of errors in pixel classification due to the presence of bank vegetation, wet ground, or other complicating factor would be less for larger rivers. Additionally, improvement in pixel classification schemes and the effect of averaging over long reaches have the potential for further reducing error associated with the remote measurement of river width.

For large numbers of discharge measurements, the aggregate or mean measurement error may be relatively small (less than 20%), as indicated by the mean error for the single channel and braided channel estimates shown in Table 3. Thus the general task of model improvement is to reduce the standard error of the estimates so that the error associated with an individual measurement can be reduced. This would be accomplished by incorporating additional site-specific information into the prediction equations. This information could be incorporated through development of channel typing schemes (as indicated in this study) and by developing methods to use specific geomorphic features of rivers as prediction variables.

6. Discussion and conclusions

This analysis indicates that relatively accurate estimates of in-bank river discharge can be made from remote observations of water-surface width in rivers provided two channel characteristic variables are also known, the maximum channel width and the channel slope. The accuracy of the discharge estimates reported in Tables 1 and 2 indicate that calibration procedures are necessary to successfully develop discharge estimates from imagery and other remotely sensed information. Thus, development of robust calibration functions is critical to the general application of this method. After calibration, the mean accuracy of the estimates can be expected to be within

10% of the observed discharge, and the standard deviation of the error within a factor of 1.5–2.

This level of accuracy suggests that remote estimates of discharge would be most useful in regional or continental scale studies where the accuracy of the aggregate is more important than at specific locations, or where data is lacking and an estimate with a known range of expected error would enable quantification of discharge within a statistical framework. Additionally, calibration techniques may improve such that better accuracy is achieved and the range of potential applications increases. As data sets of remotely sensed water-surface widths and velocities are obtained and associated with characteristic geomorphic features including general channel type, maximum channel width and channel slope, more robust calibration methods can be developed.

Considering that traditional ground-based, non-contact discharge measurements (e.g. the slope–area method) may provide an expected accuracy in the range of $\pm 20\%$, the mean estimate accuracy potentially provided from remotely sensed information is certainly comparable. Although discharge estimates made from aerial or satellite sensed information will likely never provide the level of accuracy that can be achieved from direct in-stream measurement of depth, velocity and width (using the velocity–area method), there are numerous applications for remote discharge estimates. Where data gaps in flow records exist, in rivers that have poor accessibility, and where costs for obtaining ground-based discharge are high, satellite and aerial platforms can be used to supplement the ground-based network. In addition, because of the potential for global coverage by satellites, relatively frequent and accurate estimates of discharge over large areas can provide much needed understanding of the spatial distribution of discharge across the continents on a near-real-time basis.

The necessary data to estimate discharge can all be obtained from remote sources (maps, digital elevation models and aerial or satellite images). However, it may be difficult to automate or readily obtain the maximum (bankfull) channel width, especially considering that a certain amount of judgment is required to define the maximum areal extent of the active channel. Assuming that the channel dimensions and the channel slope are relatively constant (at least over a period of years), inventories of this information can be developed from air photo and map analysis, and from field surveys. This data can then serve as baseline information that is coupled with dynamic tracking of water-surface width to obtain time series estimates of river discharge over large areas or selected sets of rivers.

Another approach to defining the maximum channel width of rivers would be based on accumulated water-surface width measurements developed over time. Similar to the braided river channel, a sufficiently long time series of widths would enable the maximum channel width to be identified and catalogued. This approach would be preferable to methods that rely on the identification of the active channel from morphologic features, because the water is easier to identify. Additionally, identification of water-surface areas and widths can be automated depending on the type of imagery (for example, color infrared, SAR and panchromatic) because water can be readily distinguished from surrounding land.

The successful use of SAR imagery to simultaneously observe water-surface width and velocity holds promise as a unique tool for substantially improving the accuracy of river discharge estimates, especially when coupled with maximum channel width and channel slope information. Surface velocity measurements require information about surface wind speed and direction, in order to adequately correct the estimate for these effects. For rivers in deep gorges one can generally assume that the wind will blow in the direction of the river banks and ameliorate this restriction. An additional limitation, whereby river flow orthogonal to the radar line-of-sight results in extreme radial velocities, may be addressed by flying lines that cross the river from alternate directions and deriving the vector velocities by assuming as we have here that the flow is parallel to the banks or by combining from directionally diverse paths. A further preferable alternative is a system that is able to measure velocity in a single pass by having directionally diverse multi-beam interferometric measurement capability (Moller et al., 2002; Frasier and Camps, 2001).

The equations developed by Bjerklie et al. (2003) indicate that discharge estimating models that include width, depth and slope have generally greater accuracy, especially for larger rivers, compared to models that use width and slope only, or width, slope

and velocity. Inclusion of remotely observed stage (water-surface elevation) from altimetry (Birkett, 1998) may provide an additional dynamic variable that can be used to estimate the depth and thus improve the accuracy of estimates even further. The accuracy of current generation altimeters such as those deployed on TOPEX/Posieden and ERS-1 and 2 is approximately 10–50 cm (Birkett, 1998), however there is the potential for higher accuracy using laser altimeters such as GLAS (NASA, 1997). Depth estimates could be developed from stage given knowledge of the river bottom or top-of-bank elevation, or from time series of stage observations over a range of water levels.

Observation of water-surface area (and width) and river channel characteristics can be made, with currently operating satellites, frequently and over much of the globe on a routine basis from a variety of sensors (Bjerklie et al., 2003). However, surface velocity and stage data may be available only on an occasional basis depending on the orbits of satellites, sensor capabilities and availability. In these circumstances more accurate discharge estimates could be made when these data are available. Discharge ratings could then be developed that relate the routinely made estimates based on measured widths and map slopes to those made using additional velocity and/or stage observations. This approach would maximize the use of the more readily available data (water-surface area and channel slope) and enable less available data (surface velocity and stage) to be successfully incorporated into a river discharge observing strategy.

Acknowledgements

Elements of this research were funded by NASA grant numbers NAG5-7601 and NAG5-8683. The Missouri River radar work described in this paper was carried out by the Jet Propulsion Laboratory (JPL), California Institute of Technology under contract with the National Aeronautics and Space Administration (NASA). We would like to acknowledge Ernesto Rodriguez, JPL, for his guidance and feedback regarding the analysis of the Missouri River AirSAR imagery, and Charles J, Vörösmarty, Institute for the Study of Earth, Oceans and Space at the University of New Hampshire for providing guidance, insight and ideas which contributed to this work.

References

Alsdorf, D., Lettenmaier, D., Vörösmarty, C.J., 2003. The need for global satellite-based observations of terrestrial surface waters. EOS Trans. AGU 84 (269), 275–276.

Barnes, H.H., 1967. Roughness characteristics of natural channels. USGS Water Supply Paper 1849, pp. 213.

Birkett, C.M., 1998. Contribution of the TOPEX NASA radar altimeter to the global monitoring of large rivers and wetlands. Water Resour. Res. 34 (5), 1223–1239.

Birkett, C.M., Mertes, L.A.K., Dunne, T., Costa, M.H., Jasinski, M.J., 2002. Surface water dynamics in the Amazon Basin: application of satellite radar altimetry. Presentation Second International LBA Scientific Conference, Manaus, Amazonas, Brazil, July 7–10.

Bjerklie, D.M., Lawrence Dingman, S., Vorosmarty, C.J., Bolster, C.H., Congalton, R.G., 2003. Evaluating the potential for measuring river discharge from space. J. Hydrol. 278 (1–4), 17–38.

Bragg, W.L., 1913. The diffraction of short electromagnetic waves by a crystal. Proc. Cambridge Phil. Soc. 17, 43.

Brakenridge, G.R., Knox, J.C., Paylor, E.D., Magilligan, F.J., 1994. Radar remote sensing aids study of the Great Flood of 1993. Am. Geophys. Union EOS Trans. AGU 75 (45), 521–527.

Brakenridge, G.R., Tracy, B.T., Knox, J.C., 1998. Orbital SAR remote sensing of a river flood wave. J. Remote Sensing 19 (7), 1439–1445.

Bray, D.I., 1979. Estimating average velocity in gravel-bed rivers. J. Hydraulic Div. ASCE HY9 1979;, 1103–1123.

Coon, W.F., 1998. Estimation of roughness coefficients for natural stream channels with vegetated banks. US Geological Survey Water Supply Paper 2441, pp. 133.

Costa, J.E., Spicer, K.R., Cheng, R.T., Haeni, E.P., Melcher, N.B., Thurman, E.M., 2000. Measuring stream discharge by non-contact methods: a proof of concept experiment. Geophys. Res. Lett. 27 (4), 553–556.

Dingman, S.L., 1984. Fluvial Hydrology. W.H. Freeman, New York, p. 383.

Ferguson, R.I., 1986. Hydraulics and hydraulic geometry. Prog. Phys. Geogr. 10 (1), 1–31.

Frasier, S.J., Camps, A.J., 2001. Dual-beam interferometry for ocean surface current vector mapping. IEEE Trans. Geophys. Remote-sensing 39 (2), 401–414.

Goldstein, R.M., Barnett, T.P., Zebker, H.A., 1989. Remote Sensing of Ocean currents. Science 246, 1282–1285.

Henderson, F.M., 1966. Open Channel Flow. MacMillan, New York.

Hicks, D.M., Mason, P.D., 1991. Roughness Characteristics of New Zealand Rivers, New Zealand DSIR Marine and Freshwater Resources Survey, Wellington, NZ 1991, p. 329.

Horritt, M.S., Mason, D.C., Luckman, A.J., 2001. Flood boundary delineations from synthetic aperture radar imagery using a statistical active contour model. J. Remote Sensing 22 (13), 2489–2507.

IAHS Ad Hoc Committee, 2001. Global water data: a newly endangered species, EOS transactions. American Geophysical Union 82 (5), 54, 56, 58.

Kinsman, B., 1965. Wind Waves. Prentice-Hall, Englewood Cliffs, NJ.

Koblinsky, C.J., Clarke, R.T., Brenner, A.C., Frey, H., 1993. Measurement of river level with satellite altimetry. Water Resour. Res. 29 (6), 1839–1848.

Kuprianov, V.V., 1978. Aerial methods of measuring river flow, in: Herschy (Ed.), Hydrometry: Principles and Practices, first ed. Wiley, Chichester, pp. 473–478.

Lacey, G., 1946–47. A general theory of flow in alluvium. J. Inst. Civil Eng., London, England 27, 16–47 (Paper No. 5518).

Leopold, L.B., 1994. A View of the River. Harvard University Press, London, England.

Leopold, L.B., Wolman, M.G., Miller, J.P., 1964. Fluvial Processes in Geomorphology. W.H. Freeman, New York.

Manning, R., 1889. On the flow of water in open channels and pipes. Transactions of the Institution of Civil Engineers of Ireland 20, 161–207.

Moller, D.K., Pollard, B., Rodriguez, E., 2002. Feasibility study for a spaceborne along-track interferometer/scatterometer, 2002 AirSAR Workshop Proceedings.

NASA Earth Observing System GLAS Science Team, 1997. Anon., 1997. Geoscience Laser Altimeter System (GLAS) Science Requirements, ICES-UTA-SPEC-001,GLAS-UTA-REQ-001 1997.

Rantz, S.E., et al., 1982. Measurement and computation of streamflow: volume 1 measurement of stage and discharge. US Geological Survey Water Supply Paper 2175.

Rosgen, D.L., 1994. A classification of natural rivers. Catena 1994;, 169–199.

Sauer, V.B., Meyer, R.W., 1992. Determination of error in individual discharge measurements. US Geological Survey Open-File Report 92-144.

Smith, L.C., 1997. Satellite remote sensing of river inundation area, stage, and discharge: a review. Hydrological Processes 11, 1427–1439.

Smith, L.C., Isacks, B.L., Bloom, A.L., Murray, A.B., 1996. Estimation of discharge from three braided rivers using synthetic aperture radar satellite imagery. Water Resour. Res. 32 (7), 2021–2034.

US Geological Survey, 2001. NWIS Streamflow Measurement Data Base, www.water.usgs.gov/nwis/measurements

Vörösmarty, C.J., Birkett, C., Dingman, L., Lettenmaier, D.P., Kim, Y., Rodriguez, E., Emmitt, G.D., Plant, W., Wood, E., 1999. NASA post-2002 land surface hydrology mission component for surface water monitoring, HYDRA_SAT. A report from the NASA Post 2002 LSHP Planning Workshop, Irvine CA, April 12–14, pp. 53.